ORIGINAL PAPER

Improved estimation of ligand–macromolecule binding affinities by linear response approach using a combination of multi-mode MD simulation and QM/MM methods

Akash Khandelwal · Stefan Balaz

Abstract Structure-based predictions of binding affinities of ligands binding to proteins by coordination bonds with transition metals, covalent bonds, and bonds involving charge re-distributions are hindered by the absence of proper force fields. This shortcoming affects all methods which use force–field-based molecular simulation data on complex formation for affinity predictions. One of the most frequently used methods in this category is the Linear Response (LR) approach of Åquist, correlating binding affinities with van der Waals and electrostatic energies, as extended by Jorgensen's inclusion of solvent-accessible surface areas. All these terms represent the differences, upon binding, in the ensemble averages of pertinent quantities, obtained from molecular dynamics (MD) or Monte Carlo simulations of the complex and of single components. Here we report a modification of the LR approach by: (1) the replacement of the two energy terms through the single-point QM/MM energy of the time-averaged complex structure from an MD simulation; and (2) a rigorous consideration of multiple modes (mm) of binding. The first extension alleviates the force-field related problems, while the second extension deals with the ligands exhibiting large-scale motions in the course of an MD simulation. The second modification results in the correlation equation that is nonlinear in optimized coefficients, but does not lead to an increase in the number of optimized coefficients. The application of the resulting mm QM/MM LR approach to the inhibition of zinc-dependent gelatinase B (matrix metalloproteinase 9) by 28 hydroxamate ligands indicates a significant improvement of descriptive and predictive abilities.

Dedicated to Yvonne C. Martin on the occasion of her round birthday and retirement

A. Khandelwal · S. Balaz (✉)
Department of Pharmaceutical Sciences, College of Pharmacy, North Dakota State University, Sudro Hall Suite 8, Fargo, ND 58105, USA
e-mail: stefan.balaz@ndsu.edu

Introduction

The continuously growing number of protein structures and protein structural models, resulting from the knowledge of genomes, represents enormous promise for development of drugs and other bioactive compounds. Full utilization of the potential requires an armory of computational methods for prediction of ligand–protein binding affinities. Structure-based prediction methods with various levels of accuracy and speed are available today: fast docking and scoring approaches [1, 2] for reduction of vast chemical libraries to several hundreds of probable binders, the second-pass methods selecting a dozen or so compounds with a high probability of success, and the most sophisticated methods like Free Energy Perturbation [3] and Thermodynamic Integration [4], which can e.g., discern the affinity of closely related analogs.

In recent years, most developments have been seen in the second category of methods, which are based on decomposition of the binding free energy. The methods usually use conformational sampling of the ligand–receptor complex and of free reactants by Molecular Dynamics (MD) or Monte Carlo (MC) simulations, although the use of multiple structures corresponding to energy minima [5] or single optimized structures to speed up the calculations have also been advocated [6, 7]. Other differences appear in the following areas: the treatment of solvent (explicit [8], continuum [6, 9], or in vacuo [6, 10]), estimation of the electrostatic component of solvation energies (linearized Poisson–Boltzman equation [5, 6, 10–13], the generalized Born model [9, 12, 14], or the pair-wise Coulomb relations in explicit solvent [15]), and the parameter optimization (used [16] or not used [5, 13]).

We prefer to use Linear Response (LR) method [8] and, especially, its extended variant [17], because they contain 3–5 adjustable coefficients, which, in our opinion, account for the differences between the simulated and experimental systems better than other approaches. The LR decomposition of the free energy of binding, ΔG_b, reads:

$$\begin{aligned} \Delta G_b &= -RT \ln K = \alpha \, \Delta\langle E\rangle + \gamma \, \Delta\langle PSA\rangle \\ &\quad + \delta \, \Delta\langle NPSA\rangle + \kappa \end{aligned} \tag{1}$$

where K is the association constant, R is the universal gas constant, T is temperature, E denotes the energy (van der Waals energy and electrostatic energy, scaled by separate coefficients α and β [8, 17] or overall QM/MM energy scaled by α [18]), PSA and $NPSA$ represent polar and nonpolar solvent-accessible surface areas [17], and γ, δ, and κ are adjustable coefficients. The angle brackets denote the ensemble averages and Δ indicates the difference between the ensemble averages in the bound and free ligand states. The ensemble averages of the energies and the surface areas can be replaced by the respective quantities calculated for the time-averaged structures [10].

The MD simulations are often trapped in local minima close to the starting conformations. To obtain a better sampling of the conformational space, strategies as replica exchange MD [19] or local replica exchange MD [20] were devised. Alternatively, predominant states can be analyzed as in the approach called Mining Minima [21]. Some ligands exhibit extensive movements and need much longer MD simulations to equilibrate than the rest of compounds. To reduce the cost, these ligands can be included in the LR correlations by treating them as assuming several binding modes, as described in our multi-mode (mm) approach [22].
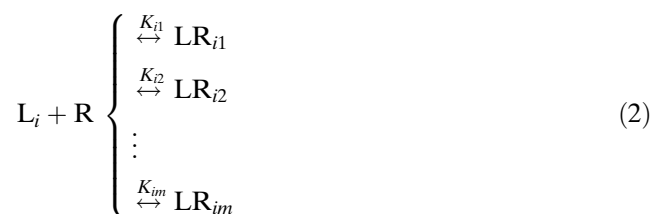
A natural question emerges, whether the QM/MM energies can also be successfully used in the mm approach. To examine this possibility, the mm QM/MM LR method was applied to a set of 28 diverse hydroxamate inhibitors [23] of gelatinase B (MMP-9), a member of the family of matrix metalloproteinases (MMPs). MMPs participate in remodeling of extracellular matrix and are implicated in cancer, metastases, arthritis, and other diseases [24].

Background and methods

To provide the theoretical background for the correlation equation underlying the mm QM/MM LR approach, the description of binding equilibria as well as the replacement of the ensemble averages of van der Waals and electrostatic energies are briefly reviewed. The computational protocol is described.

Multi-mode binding equilibria

Reversible 1:1 binding of the i-th ligand L_i in m mutually exclusive orientations or conformations (modes) to the receptor site R can be schematically written as

$$L_i + R \begin{cases} \overset{K_{i1}}{\leftrightarrow} LR_{i1} \\ \overset{K_{i2}}{\leftrightarrow} LR_{i2} \\ \vdots \\ \overset{K_{im}}{\leftrightarrow} LR_{im} \end{cases} \tag{2}$$

Individual equilibria are characterized by the partial association constants K_{ij}. The ligand is present as a single species in the receptor surroundings. The apparent association constant K_i for this process is, on the concentration basis, defined as

$$K_i = \sum_{j=1}^{m} \left[LR_{ij}\right] / \left([L_i]\,[R]\right) = \sum_{j=1}^{m} K_{ij}. \tag{3}$$

Equation (3) is in accordance with the Mining Minima approach to calculation of free energies [5], as well as with other published analyses of formally analogous situations: the rigorous statistical thermodynamic description [25] and equilibrium treatment [26, 27] of the multi-mode interactions of ligands with proteins, and kinetic analyses of reversible uni-molecular reactions leading to different products [28] or isomers [29].

Each partial association constant K_{ij} can be expressed using Eq. (1), with the same values of the

adjustable coefficients α, β, γ, δ and κ. The apparent association constant K_i can then be correlated with the simulation results by a combination of Eq. (1), now with the subscript ij representing the j-th binding mode of the i-th compound), and Eq. (3):

$$\ln K_i = \ln \sum_{j=1}^{m} \exp\left[- \left(\alpha \ \Delta\langle E \rangle_{ij} + \gamma \ \Delta\langle PSA \rangle_{ij} \right. \right.$$
$$\left. \left. + \delta \ \Delta\langle NPSA \rangle_{ij} + \kappa \right)/RT \right]. \quad (4)$$

In addition to predicting the binding affinity, Eq. (4) can also select the most dominant bound conformation(s) of the ligand out of the set of hypothetical conformations. Individual exponentials in Eq. (4) represent the partial association constants K_{ij} of binding modes as defined in Eqs. (2) and (3). After the coefficients in Eq. (4) are optimized, the Boltzmann probability of each bound conformation is easily calculated as $K_{ij}/\Sigma K_{ij}$.

The QM/MM binding energy

The use of molecular mechanics (MM) for the description of the ligand–receptor interactions requires similarity of chemical bonds in free and bound systems. Once the bonds change upon binding, most commonly when covalent or coordination bonds are formed or even when polarizability causes a different charge distribution for ligand–receptor complex, the use of standard force fields becomes problematic. Two possible solutions to this problem are represented by the development of more sophisticated force fields or by the use of quantum mechanical (QM) methods. For large ligand–receptor systems, combination QM/MM methods are frequently used, with the QM domain including the changing bonds and the MM domain covering the rest of the receptor molecules.

The use of the time-averaged structures in place of the ensemble averages in the LR equations makes the use of QM/MM methods straightforward: the energy of the relaxed time-averaged structures can be used instead of the van der Waals and electrostatic energies in Eq. (1). We have recently shown that this modification of the LR approach with electrostatic and van der Waals energies improves both descriptive and predictive abilities of the correlation [18].

Computational protocol

The computation details were described previously [18, 22]. Briefly, the protocol consisted of: (1) FlexX docking of the ligands to the processed structure of MMP-9 taken from the Protein Data Bank [30] (file

1GKC [31]), with the pose selected primarily on the basis of acceptable distances between the catalytic zinc and the hydroxamate atoms; (2) QM/MM minimization of the selected poses, with the QM region including the ligand, tha catalytic zinc, Glu402 and the His triad as shown in Fig. 1; (3) 200-ps MD simulation of the complex with the zinc bonds restricted; and (4) calculation of single-point QM/MM energies of the complex in the time-averaged structures from the simulations.
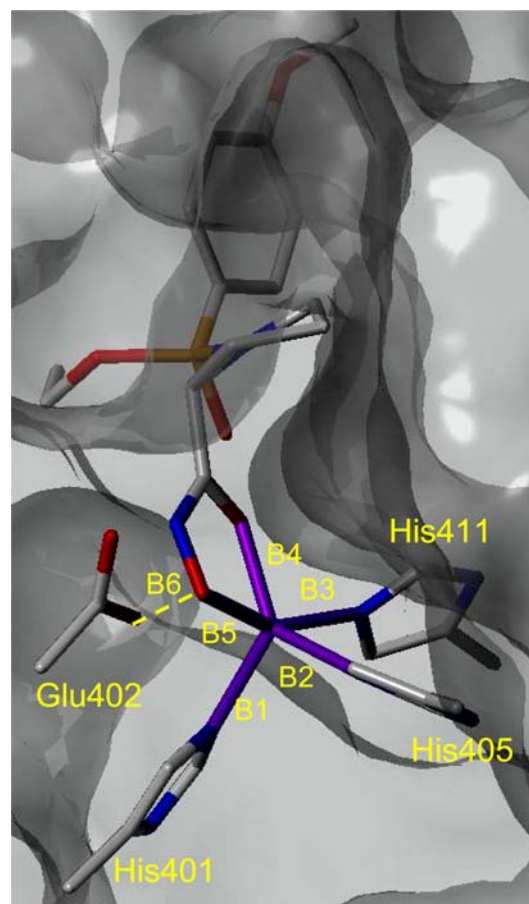

Fig. 1 The average lengths and standard deviations (Å) of the bonds (in magenta) between Zn and coordinating atoms: B1 = 2.120 ± 0.022, B2 = 2.156 ± 0.011, B3 = 2.253 ± 0.016, B4 = 2.029 ± 0.018, and B5 = 2.089 ± 0.012 for all studied compounds. The hydrogen-bond lengths between Glu402 and O1 of the hydroxamate group were characterized by B6 = 2.604 ± 0.065. The average bond angles O1–Zn–N in His401, His405 and His411 are 121.77 ± 14.81°, 135.58 ± 8.95°, and 82.06 ± 1.65°, respectively. The average bond angles O2–Zn–N in the same order are 101.55 ± 1.89°, 95.07 ± 2.13°, and 155.23 ± 2.98°, respectively. The average bond angle of O2–Zn–O1 is 79.66 ± 0.61. The smallest inhibitor **28** (Table S1, supplementary information) shown in the time-averaged position after 200-ps MD simulations. The surface of the MMP-9 is shown in gray

The van der Waals, electrostatic energies, and surface area terms were calculated using the corresponding time-averaged structures of the complex and the free ligand for eight 25-ps intervals of the 200-ps MD simulations. The time-averaged structure for each interval represented a binding mode: 0–25 ps—mode 1, 25–50 ps—mode 2,... 175–200 ps—mode 8. The structures of the compounds and inhibitory activities, both experimental [23] and calculated by individual equations, are given in supporting information (Table S1).

Results and discussion

The QM/MM optimization of the best FlexX poses showed that the hydroxamate groups of all 28 derivatives created, along with the histidine triad of MMP-9, rather similar trigonal bipyramidal coordination spheres around the catalytic zinc [18] (Fig. 1). Glu402 formed the hydrogen bonds with the nonionized hydroxyl group of the hydroxamates. The QM/MM approach, in general, handles the zinc–ligand charge transfer, bond length changes, polarization, and ionization of the ligands upon binding to zinc better than advanced force fields.

The ligand behavior differed more in the 200-ps simulations following 100-ps equilibrations with harmonically restrained zinc-binding groups (Fig. 2). Most ligands were well equilibrated (as ligand **27**, structure in Table S1 in supplementary information), but some ligands showed large-scale motions (e.g., ligands **22** and
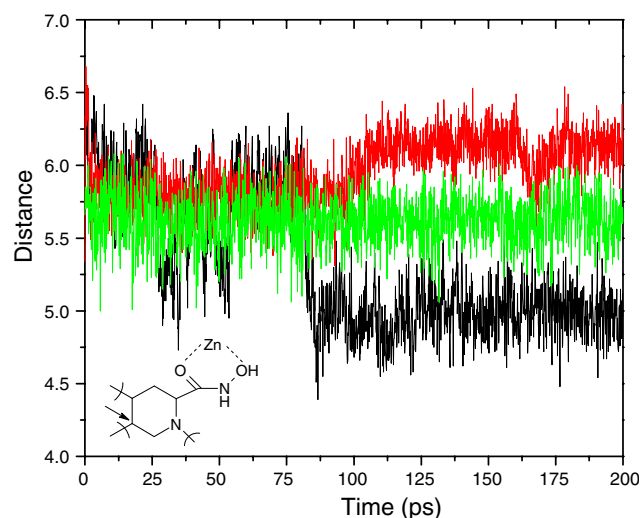

Fig. 2 The distance (Å) between Zn and the carbon atom indicated by the arrow for compounds **7** (black), **22** (red), and **27** (green) throughout the MD simulation. Structures of studied compounds are given in Table S1 in supplementary information

especially **7**). The multi-mode approach was implemented to account for the instabilities. The LR terms in Eqs. (1) and (4), which were calculated for the minimized and time-averaged structures from the MD data (supplementary information, Tables S2 and S3, respectively) did not exhibit colinearities: the highest mutual correlation coefficient was $r^2 = 0.193$. As the last parameter, the single-point QM/MM energies for the time-averaged structures resulting from the 200-ps MD simulations were calculated. In all studied cases, the used time-averaged structures were close to at least one structure recorded in the simulation.

All statistically significant results of the fits of Eqs. (1) and (4) to the data for the one-mode and multi-mode LR approaches with classical and QM/MM energy parameters are summarized in Table 1. In all cases, the dependent variable was $\ln(1/K_i)$ because the reported K_i values [23] are the inhibition constants, not the association constants. The quality of individual fits can be assessed using the statistical indices in Table 1 and also the plot of residuals vs. the experimental activities for individual equations (Fig. 3). The FlexX docking, while providing good starting geometries, did not allow the FlexX scoring function to discriminate between individual binding affinities. For both MM and QM/MM minimizations (Eq. (1), lines 2 and 3 in Table 1), the QM/MM, van der Waals, and electrostatic terms were statistically not significant and the coefficient errors were higher than the optimized coefficient values. Moreover, the coefficients for the QM/MM and van der Waals terms had negative values. The optimized structures, regardless whether obtained by MM or QM/MM minimization, probably did not represent well the bound conformations and the results were discouraging ($r^2 = 0.508$ and 0.514), in contrast to other reports [7].

Both MD and MD + QM/MM one-mode treatments resulted in the same equation (line 4 in Table 1), because all the energy-related coefficients were insignificant. The coefficient errors for the electrostatics and *PSA* terms were almost equal to the optimized coefficient values. The sign of the coefficient for the van der Waals term was negative and the error was higher than the coefficient. Inclusion of the statistically insignificant terms led to negligible or moderate improvements in the correlations: for MM minimization, $r^2 = 0.516$; for QM/MM minimization, $r^2 = 0.520$; and for the one-mode treatment, $r^2 = 0.625$ (MD) and $r^2 = 0.630$ (MD + QM/MM). Conformational sampling using 200-ps MD simulations did not improve the statistics significantly ($r^2 = 0.589$). We showed previously [18, 32] that these correlations can be amended by a careful selection of the used intervals of MD simulations.

Table 1 Optimized coefficients and statistical indices of correlation equations

Eq.	Sampling	[a] $\alpha \times 10^{-2}$	[b] $\beta \times 10^{-2}$	$\gamma \times 10^{-2}$	$\delta \times 10^{-2}$	κ	SD	r^2	RMSE LOO[c]	LSO[d]
-	FlexX[e]	0.161 ± 0.146	NA [f]	NA	NA	-13.43 ± 4.598	2.224	0.044	2.278	2.294
1	MM minimization	NS[g]	NS	3.841 ± 1.854	1.450 ± 0.377	-9.582 ± 2.297	1.627	0.508	1.727	1.733
1	QM/MM minimization	NS	NA	3.815 ± 1.573	2.380 ± 0.634	-7.552 ± 2.236	1.618	0.514	1.712	1.795
1	MD + QM/MM (200 ps)[h]	NS	NS/NA	NS	1.824 ± 0.299	-13.59 ± 0.840	1.458	0.589	1.539	1.506
4[i]	MD (8 × 25 ps)	1.142 ± 0.784	0.721 ± 0.642	2.124 ± 1.015	1.564 ± 0.235	-6.275 ± 1.244	0.956	0.844	1.031	1.075
4[j]	MD + QM/MM (8 × 25 ps)	0.389 ± 0.076	NA	3.161 ± 0.682	1.492 ± 0.172	-6.401 ± 0.945	0.730	0.905	0.817	0.827

[a] Characterizes QM/MM interaction energy in Eq. (4) or van der Waals energy in Eq. (1)

[b] Characterizes electrostatic energy [Eq. (1)]

[c] Leave-one-out cross-validation

[d] Leave-several-out cross-validation: random selection of 6-member test set, repeated 200 times

[e] The correlation between $\ln(1/K_i)$ and the FlexX scores, with the slope α and the intercept κ

[f] NA—not applicable

[g] NS—non-significant coefficient

[h] These results are valid for both MD and QM/MM energies (LR and QM/MM LR approaches), because none of the energy terms was significant

[i] The mm LR approach

[j] The mm QM/MM LR approach
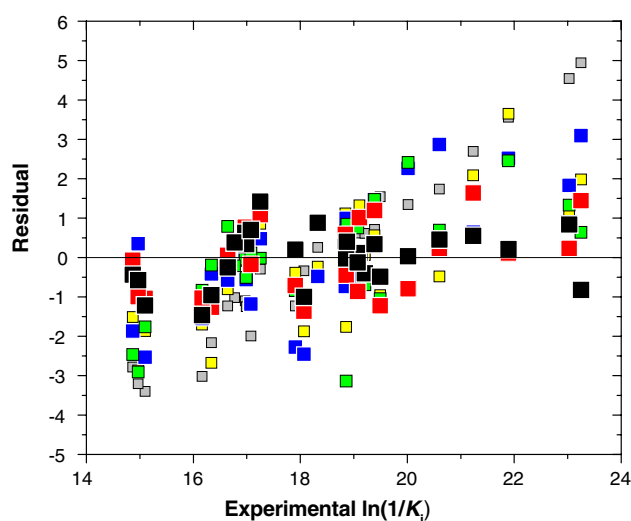
Fig. 3 Plot of residuals (experimental minus calculated activities) obtained from FlexX docking (grey), MM minimization (yellow), QM minimization (blue), LR and QM/MM LR approach (green), mm LR approach (red), and mm QM/MM LR approach (black) versus experimental activity (K_i is in M). The coefficients and statistical indices for individual approaches are summarized in this order in Table 1

The interval selection is automated in the multi-mode approaches resulting in Eq. (4), which provide a real breakthrough in the performance, explaining 84% of the variance with the MD energy parameters, and 90% with the QM/MM parameter (Table 1, the last two lines). The improvement caused by the inclusion of the QM/MM energies into the multi-mode LR approach is significant and results in the best description of the data. All three terms included in Eq. (4) for the mm QM/MM LR approach exhibited significant contributions to the correlation. The residuals (Fig. 3) are the lowest among the used approaches, and seem to be randomly distributed.

The robustness of the regression Eqs. (1) and (4) and their predictive abilities were probed by leave-one-out (LOO) and leave-several-out (LSO) cross-validation procedures. The latter approach, using a random selection of a six-member test set that was repeated 200 times, provided a thorough evaluation. The predictivity of the mm QM/MM LR approach is better than with other approaches (Table 1, the last line). The RMSE values using LOO (0.817) and LSO (0.827) cross-validations were comparable to the SD value (0.730), which is equivalent to the RMSE value without any compound omission.

The prevalences of individual simulation intervals representing the binding modes for the studied ligands can be calculated as $K_{ij}/\Sigma K_{ij}$, where the partial association constants K_{ij}, as defined in Eqs. (2) and (3), correspond to individual exponentials in Eq. (4). The prevalences are summarized in Table S4 in the supporting information, and plotted against inhibitory activities in Fig. 4. Apparently, the number of binding modes is not related to the activity, contrary to the
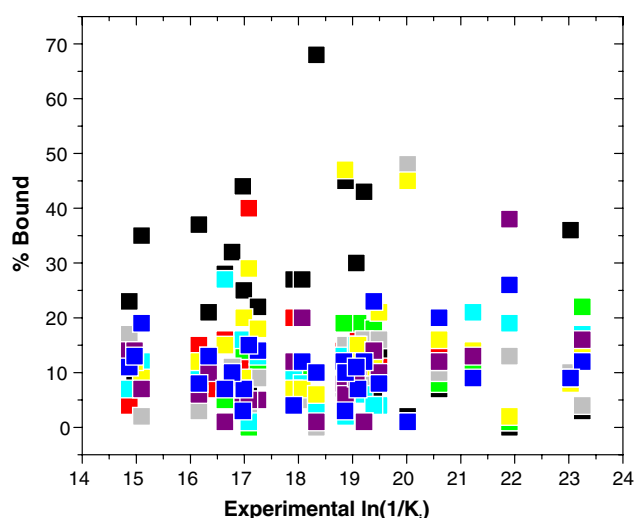
Fig. 4 Plot of prevalencies of individual modes versus experimental $\ln(1/K_i)$ values, calculated from the best mm QM/MM LR correlation (the last line in Table 1). Individual modes m1–m8, representing time-averaged structures for consecutive 25-ps MD simulations, are shown in black, red, green, gray, cyan, yellow, purple, and blue colors, respectively

notion that weak binders have a frustrated energy landscapes leading to multiple binding modes [33]. It should be noted, however, that the least active compound **28** (structure in Table S1 in the supporting information) does not have a clearly dominating mode, and all the modes exhibit about equal (10–14%) contributions to the binding. All but one compounds have the major binding mode representing less than 50% of bound molecules. In 60% of the cases, mode 1 is the dominant binding mode. Major outliers in one-mode treatment (compounds **2**, **3**, **6**, **15**, **21**, **22**, **25**, and **28**, Table S1 in the supporting information) are predicted accurately by the multi-mode treatment.

The presented mm QM/MM LR approach, combining MD simulations and QM/MM methods, exhibits very good descriptive and predictive abilities for the studied inhibition of MMP-9 by hydroxamate ligands. If further studies confirm the applicability of the approach, it can become a useful addition to the armory of the approaches to the structure-based prediction of binding affinities. The two novel features of the mm QM/MM LR approach become especially handy in the following situations. The multi-mode treatment automates the selection of suitable simulation intervals for compounds undergoing significant large-scale movements. The QM/MM energy provides superior descriptions of the binding energies if the ligand–macromolecule complex is formed by coordination, covalent or polarizable bonds rather than by standard weak interactions.

References

1. Muegge I, Rarey M (2001) Rev Comput Chem 17:1
2. Leach AR, Shoichet BK, Peishoff CE (2006) J Med Chem 49:5851
3. Kollman P (1993) Chem Rev 93:2395
4. van Gunsteren WF (1989) In: van Gunsteren, Weiner PK (eds) Computer simulation of biomolecular systems. Escom, Leiden, pp 27–59
5. Chang CE, Gilson MK (2004) J Am Chem Soc 126:13156
6. Huang D, Caflisch A (2004) J Med Chem 47:5791
7. Kuhn B, Gerber P, Schulz-Gasch T, Stahl M (2005) J Med Chem 48:4040
8. Åqvist J, Medina C, Samuelsson JE (1994) Protein Eng 7:385
9. Zhou R, Friesner RA, Ghosh A, Rizzo RC, Jorgensen WL, Levy RM (2001) J Phys Chem B 105:10388
10. Zoete V, Michielin O, Karplus M (2003) J Comput Aid Mol Des 17:861
11. Kollman PA, Massova I, Reyes C, Kuhn B, Huo S, Chong L, Lee M, Lee T, Duan Y, Wang W, Donini O, Cieplak P, Srinivasan J, Case DA, Cheatham TE (2000) Acc Chem Res 33:889
12. Srinivasan J, Cheatham TE III, Cieplak P, Kollman PA, Case DA (1998) J Am Chem Soc 120:9401
13. Kuhn B, Kollman PA (2000) J Med Chem 43:3786
14. Rizzo RC, Toba S, Kuntz ID (2004) J Med Chem 47:3065
15. Smith MBK, Hose BM, Hawkins A, Lipchock J, Farnsworth DW, Rizzo RC, Tirado RJ, Arnold E, Zhang W, Hughes SH, Jorgensen WL, Michejda CJ, Smith RH (2003) J Med Chem 46:1940
16. Tounge BA, Reynolds CH (2003) J Med Chem 46:2074
17. Carlson HA, Jorgensen WL (1995) J Phys Chem 99:10667
18. Khandelwal A, Lukacova V, Comez D, Kroll DM, Raha S, Balaz S (2005) J Med Chem 48:5437
19. Swendsen RH, Wang JS (1986) Phys Rev Lett 57:2607
20. Cheng X, Cui G, Hornak V, Simmerling C (2005) J Phys Chem B 109:8220
21. Head MS, Given JA, Gilson MK (1997) J Phys Chem A 101:1609
22. Khandelwal A, Lukacova V, Kroll DM, Raha S, Comez D, Balaz S (2005) J Phys Chem A 109:6387
23. Sawa M, Kiyoi T, Kurokawa K, Kumihara H, Yamamoto M, Miyasaka T, Ito Y, Hirayama R, Inoue T, Kirii Y, Nishiwaki E, Ohmoto H, Maeda Y, Ishibushi E, Inoue Y, Yoshino K, Kondo H (2002) J Med Chem 45:919
24. Overall CM, Kleifeld O (2006) Nat Rev Cancer 6:227
25. Wang J, Szewczuk Z, Yue SY, Tsuda Y, Konishi Y, Purisima EO (1995) J Mol Biol 253:473
26. Balaz S, Hornak V, Haluska L (1994) Chemom Intell Lab Syst 24:185
27. Hornak V, Balaz S, Schaper KJ, Seydel JK (1998) Quant Struct Act Rel 17:427
28. Jullien L, Proust A, LeMenn JC (1998) J Chem Educ 75:194
29. Smith WR, Missen RW (1982) Chemical reaction equilibrium analysis: theory and algorithms. John Wiley and Sons, New York

30. Berman HM, Westbrook J, Feng Z, Gilliland G, Bhat TN, Weissig H, Shindyalov IN, Bourne PE (2000) Nucleic Acids Res 28:235
31. Rowsell S, Hawtin P, Minshull CA, Jepson H, Brockbank SMV, Barratt DG, Slater AM, McPheat WL, Waterson D, Henney AM, Pauptit RA (2002) J Mol Biol 319:173
32. Khandelwal A, Lukacova V, Kroll DM, Comez D, Raha S, Balaz S (2004) QSAR Comb Sci 23:754
33. Rejto PA, Verkhivker GM (1996) Proc Natl Acad Sci 93:8945